Catalysis Science & Technology

PAPER

View Article Online
View Journal

Cite this: DOI: 10.1039/c4cy01566e

Catalytic oxidation of cellobiose over TiO_2 supported gold-based bimetallic nanoparticles†

Prince Nana Amaniampong,[ab] Xinli Jia,[a] Bo Wang,[b] Samir H. Mushrif,*[a] Armando Borgna*[b] and Yanhui Yang*[a]

Received 28th November 2014,
Accepted 29th January 2015

DOI: 10.1039/c4cy01566e

www.rsc.org/catalysis

A series of Au–M (M = Cu, Co, Ru and Pd) bimetallic catalysts were supported on TiO_2 *via* a deposition–precipitation (DP) method, using urea as a precipitating agent. The resulting catalysts were employed in the catalytic oxidation of cellobiose to gluconic acid and the properties of these catalysts were carefully examined using various characterization techniques. Cu–Au/TiO_2 and Ru–Au/TiO_2 catalysts demonstrated excellent catalytic activities in the oxidation of cellobiose to gluconic acid, though with contrasting reaction mechanisms. Complete conversion of cellobiose (100%) with a gluconic acid selectivity of 88.5% at 145 °C within 3 h was observed for reactions performed over Cu–Au/TiO_2; whereas, a conversion of 98.3% with a gluconic acid selectivity of 86. 9% at 145 °C within 9 h was observed for reactions performed over Ru–Au/TiO_2. A reaction pathway was proposed based on the distribution of reaction products and kinetic data. It is suggested that cellobiose is converted to cellobionic acid (4-*O*-beta-D-glucopyranosyl-D-gluconic acid) and then gluconic acid is formed through the cleavage of the β-1,4 glycosidic bond in cellobionic acid over Cu–Au/TiO_2 catalysts. On the other hand, for reactions over the Ru–Au/TiO_2 catalyst, glucose was observed as the reaction intermediate and gluconic acid was formed as a result of glucose oxidation. For reactions over Co–Au/TiO_2 and Pd–Au/TiO_2 catalysts, fructose was observed as the reaction intermediate, along with small amounts of glucose. Co and Pd remarkably promoted the successive retro-aldol condensation reactions of fructose to glycolic acid, instead of the selective oxidation to gluconic acid.

Introduction

Abundant and renewable lignocellulosic biomass is considered as a promising alternative to non-renewable petroleum-based resources. The use of second-generation biomass as a feedstock to produce fuels and chemicals is sustainable and is of great interest to help solve energy and environmental problems in the future.[1–5] Cellulose is the largest component of lignocellulosic biomass, accounting for 40–50% by mass.[2,3] Recently, extensive research to study the chemical/biological transformations of cellulose into high-value added chemicals such as gluconic acid and its derivatives has been performed since gluconic acid is an important platform chemical which is widely used in pharmaceutical applications and in the food industry as a water-soluble cleanser and additive.[6–9] Homogeneous catalysis has been widely used for the oxidation of cellulose to gluconic acid.[7–9] However, it imposes many disadvantages arising from product separation, formation of by-products and disposal of wastewater.[8] The cost of traditional fermentation processes to produce gluconic acid is high due to the system-specific requirements, *e.g.*, high temperature, high level of purification and cost of bioreactors. Hence, the development of novel heterogeneous catalysts is of great significance to provide efficient and economical alternatives to these primitive techniques.[10]

Attributed to the cohesive interactions between metal species and supports, with either Lewis or Brønsted acid sites, multifunctional catalysts have shown outstanding catalytic performance in the conversion of cellulose to gluconic acid.[11–28] However, cellulose is a very complex macromolecule and is insoluble in most solvents. Hence, it is not easy to perform fundamental research using cellulose as a feedstock. Cellobiose, which is a D-glucose dimer connected by a β-1, 4 glycosidic bond, represents the simplest model of cellulose. The studies on the catalytic conversion of cellobiose may also provide helpful clues to efficiently transform cellulose into valuable chemicals. Wang and co-workers examined the conversion of cellobiose over gold nanoparticles supported on various supports.[12] They found that the

[a] *School of Chemical and Biomedical Engineering, Nanyang Technological University, 62 Nanyang Drive, 637459, Singapore. E-mail: yhyang@ntu.edu.sg, SHMushrif@ntu.edu.sg*

[b] *Institute of Chemical and Engineering Sciences, A*STAR (Agency for Science, Technology and Research), 1 Pesek Road, Jurong Island, 627833, Singapore. E-mail: Armando_Borgna@ices.a-star.edu.sg*

† Electronic supplementary information (ESI) available: S1 XRD patterns of bimetallic catalysts studied in this work, S2 UV-vis spectra of bimetallic catalysts, and S3 NH_3-TPD of Cu–Au/TiO_2. See DOI: 10.1039/c4cy01566e

Brønsted acid sites in the carbon nanotube (CNT) had a pronounced effect on the enhancement of the hydrolysis of cellobiose to glucose, reporting a cellobiose conversion of 91%, while the presence of Au nanoparticles promoted the oxidation of glucose to gluconic acid with a selectivity of 60% at a reaction time of 3 h. This group further investigated the conversion of cellobiose over CNT-supported palladium, platinum, rhodium, copper, and silver catalysts and the best results were obtained with platinum/CNT (cellobiose conversion of 53% and gluconic acid selectivity of 23%).[12] These results revealed that the nature of the support and the type of metal catalyst played important roles in the cellobiose conversion and the selectivity towards gluconic acid.

Compared to pure metals, employing bimetallic catalysts is believed to be a promising option for biomass feedstock upgrading, as the interaction between the two metals can modify the surface and electronic properties of the catalysts, thereby enhancing significantly their catalytic activity and stability, even in the presence of undesired biomass by-products. Bimetallic Au-containing mixed metal catalysts have been developed and it has been shown that bimetallic catalysts exhibit higher catalytic activities than their monometallic analogues.[18] The effect of Cu, Co, Ru, Pt and Ni addition to a Au catalyst was studied for several reactions, including 2,3-dihydrofuran synthesis,[18] partial oxidation of methanol,[19] water-gas shift[29] and naphthalene hydrogenation.[30]

In this study, we prepared and characterized bimetallic catalysts, such as Co–Au, Cu–Au, Pd–Au and Ru–Au, supported on urea treated TiO_2 for the oxidation of cellobiose under aqueous conditions. In tune with the advantages of the catalyst preparation methods described by Zanella *et al.*,[31] we employed the deposition–precipitation method which has been proven to be an efficient method for preparing Au-based bimetallic catalysts[32–34] to obtain metallic nanoparticles with a small size of only a few nanometers. The catalytic activities of the bimetallic catalysts were then compared with those of their corresponding monometallic analogues and the influence of the second metal on the conversion of cellobiose and selectivity towards gluconic acid was studied. The aim of this work is to gain better insights into the reaction mechanisms of cellobiose conversion to gluconic acid and its derivatives over gold-based bimetallic catalysts by identifying the key intermediate compounds and also to attain better selectivity towards gluconic acid. To better understand the structure–function relationship of the catalysts, the catalyst nanoparticles were studied by X-ray diffraction (XRD), X-ray photoelectron spectroscopy, transmission electron microscopy (TEM), ammonia temperature programmed desorption (NH_3-TPD), UV-vis spectroscopy, X-ray fluorescence (XRF) and N_2 physisorption. A reaction pathway for cellobiose conversion to gluconic acid was also proposed, as shown in Scheme 1.

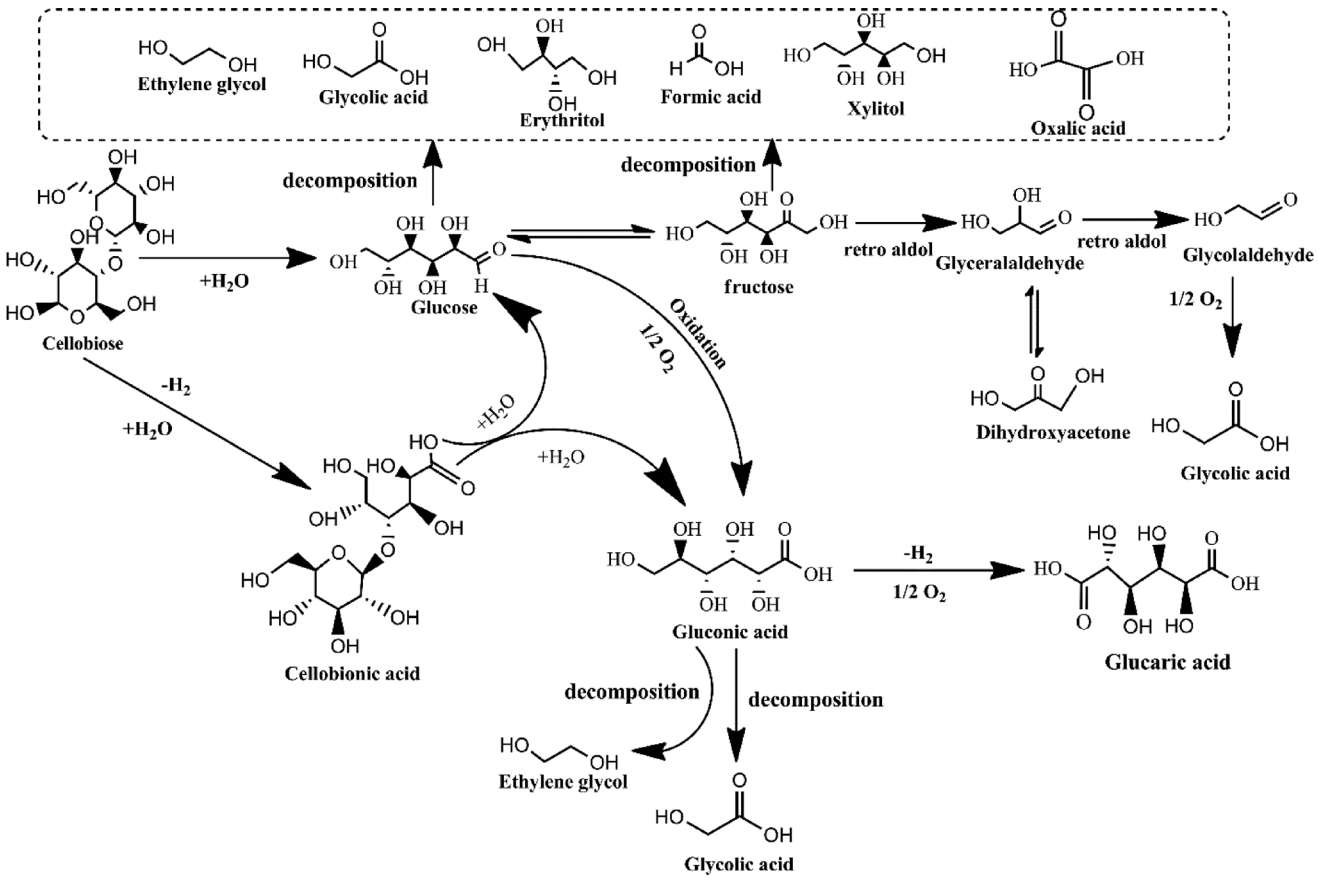

Scheme 1 Proposed reaction pathways of cellobiose conversion to gluconic acid and its derivatives.

Table 1 Structural properties of the TiO_2 support, actual metal loading and particle sizes of Au–M/TiO_2 (M = Cu, Co, Ru and Pd)

Sample	BET surface area ($m^2\ g^{-1}$)	Pore volume ($cm^3\ g^{-1}$)	Average pore size (nm)	M content[a] (wt%)	Au content[a] (wt%)	Metal particle size[b] (nm)
TiO_2	53.5	0.3	21.4	—	—	—
TiO_2 (urea treated)	54.8	0.5	33.7	—	—	—
0.5Cu–0.5Au/TiO_2	52.6	0.4	32.0	0.450	0.480	5.6
0.5Co–0.5Au/TiO_2	53.7	0.5	34.7	0.440	0.480	3.0
0.5Ru–0.5Au/TiO_2	53.6	0.5	32.5	0.350	0.488	4.6
0.5Pd–0.5Au/TiO_2	52.3	0.5	34.1	0.482	0.501	3.6
1Ru/TiO_2	52.6	0.6	36.4	0.970	—	1.5
1Cu/TiO_2	53.8	0.6	40.9	0.860	—	1.6
1Au/TiO_2	52.8	0.5	36.2	—	1.010	2.1

[a] Actual metal contents obtained from XRF analysis. [b] Metal particle size measured by TEM.

Results and discussion

Catalyst characterization

It is well known that the surface properties of a catalyst play an important role in its activity. High surface area and large pore volume favour mass transport during the reaction. Hence the textural properties of all as-prepared bimetallic samples and their monometallic analogues were also investigated.

As seen in Table 1, the pore volume of the titania support treated with urea increases slightly as compared to that of the commercial TiO_2 support without urea treatment. An earlier report[35,36] showed that urea was a good pore forming agent and as such helped in the formation of mesoporosity in the titania framework. The current study also confirms that adding urea increases the pore diameter to 34 nm, compared to 21 nm of the standard sample without urea. It is worth stating that the aim of this work is not to thoroughly investigate the effect of urea on the pore structure of the catalysts. X-ray fluorescence (XRF) analysis performed on the as-synthesized catalysts evidences that the actual metal loadings are close to the theoretical values (Table 1) and as such there is no significant loss of metal precursors during the catalyst preparation due to the effective precipitation action of the urea utilized.

The XRD characteristic peaks corresponding to palladium, gold, copper, ruthenium and cobalt are not detected for Pd–Au, Cu–Au, Ru–Au and Co–Au, respectively, because of the low amounts of metals loaded, high metal dispersion and probably, the very high intensity of the TiO_2 peaks (ESI† Fig. S1).

The particle dispersion and size distribution of both monometallic and bimetallic catalysts on the TiO_2 support are further investigated by TEM observations, as illustrated in Fig. 1. The metallic particles are finely dispersed on the support surfaces.

The monometallic Ru, Cu and Au catalysts exhibit smaller particle sizes compared to their bimetallic analogues, with an average particle size of 2.1, 1.6 and 1.5 nm for Au/TiO_2, Cu/TiO_2 and Ru/TiO_2, respectively, obtained from the TEM analysis.

For brevity, the TEM images of the monometals are not shown. Few agglomerations of the metal particles are observed for the bimetallic catalysts with average particle sizes of 3.0, 3.6, 4.6 and 5.6 nm for Co–Au/TiO_2, Pd–Au/TiO_2,

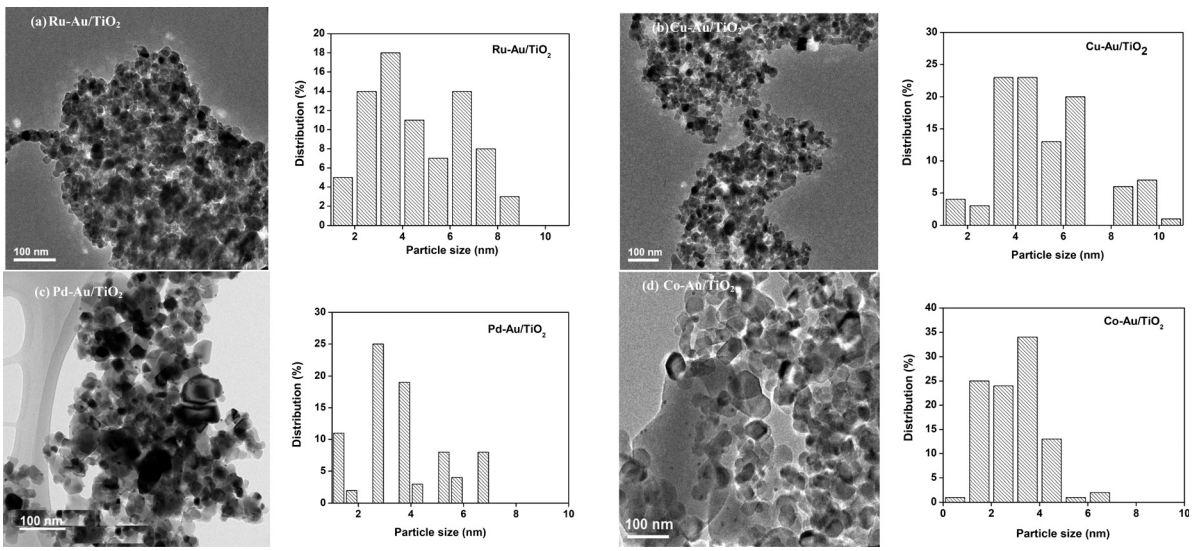

Fig. 1 Transmission electron microscopy (TEM) images of as-prepared catalysts (a) Ru–Au/TiO_2, (b) Cu–Au/TiO_2, (c) Pd–Au/TiO_2 and (d) Co–Au/TiO_2.

$Ru–Au/TiO_2$ and $Cu–Au/TiO_2$, respectively, as shown in Fig. 1a–d. The results reveal that the deposition–precipitation method using urea is indeed viable for the synthesis of metal nanoparticles with smaller size compared with other preparation methods reported in the literature.[37] Chimentão *et al.*[37] employed an impregnation method to prepare Au–Cu nanoparticles on TiO_2 and only managed to achieve a wider particle size distribution of around 5–10 nm in the case of $Au–Cu/TiO_2$ and 8–15 nm for Au/TiO_2 with large agglomerations up to 100–250 nm.

XPS spectra were recorded for the prepared catalysts and the high-resolution XPS spectra were curve fitted to evaluate the chemical states of the different species present on the surface of the TiO_2 support. The individual XPS spectrum and the corresponding binding energies (BE) of the different chemical species are shown in Fig. 2. The BE of the Au $4f_{7/2}$ line displayed in Fig. 2 was observed at around 83.0–84.6 eV for all the catalysts, indicating the presence of both reduced Au nanoparticles (metallic Au^0) and cationic nanoparticles ($Au^{\delta+}$ and Au^{3+}).

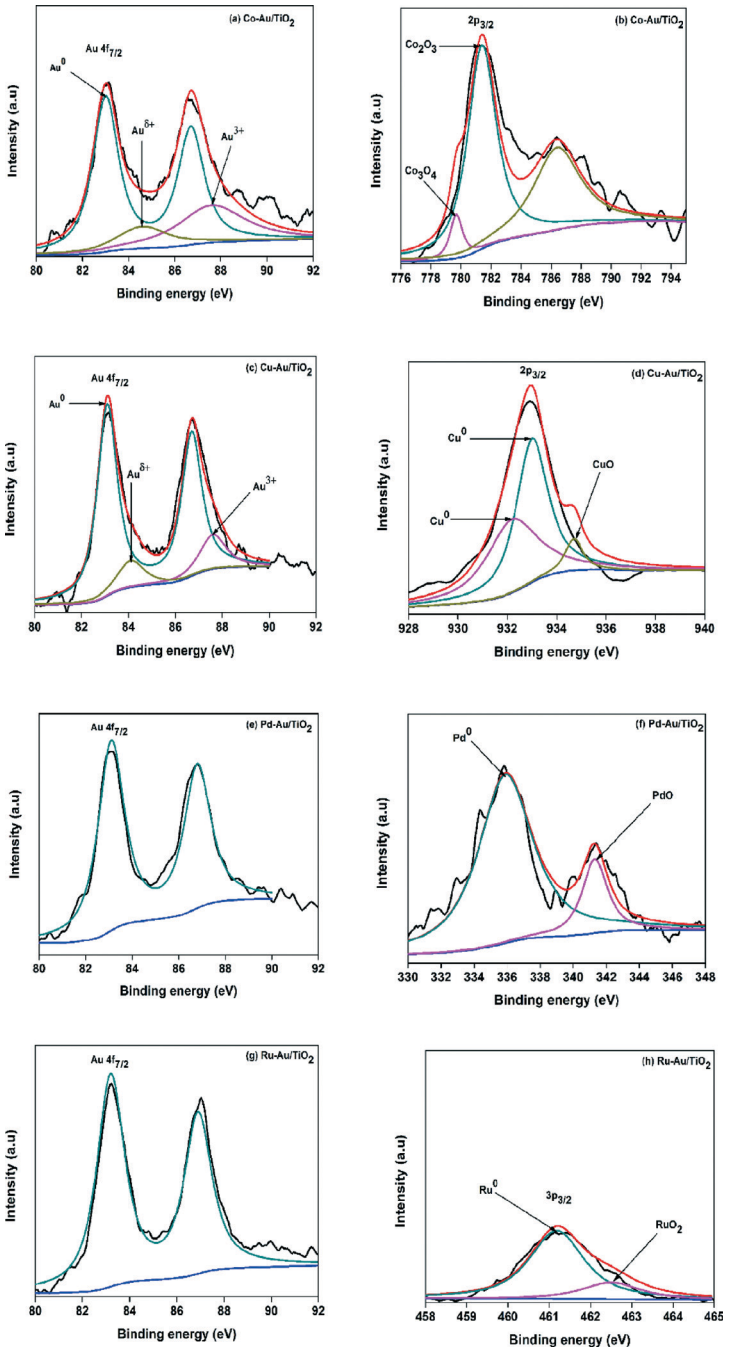

Fig. 2 X-ray photoemission spectra of as-prepared bimetallic samples.

However, in the case of Co–Au, Cu–Au, Pd–Au and Ru–Au, the significant decrease in the BE value for the Au $4f_{7/2}$ line (83.2, 83.1, 83.1 and 83.5 for Co, Cu, Pd and Ru containing catalysts, respectively) suggests that electrons are transferred from M (*i.e.*, Co, Cu, Pd and Ru) to Au atoms and these interactions of Au with Co, Cu, Pd and Ru lead to a change in the electronic structure of Au.[38]

Copper in bimetallic Cu–Au/TiO_2 exhibits peaks due to Cu $2p_{3/2}$ transitions at 932.2 eV and 933.0 eV, both of which correspond to the presence of metallic Cu on the surface of TiO_2.

In addition, the peak at 934.7 eV is indicative of CuO after calcination.

Palladium in bimetallic Pd–Au also shows characteristic peaks at around 335.9 and 341.3 eV, indicating the formation of metallic Pd and PdO on the surface of TiO_2. In the case of Co–Au/TiO_2, cobalt species display peaks at 779.7 and 781.4 eV due to the Co $2p_{3/2}$ transition, indicating the presence of two forms of cobalt species on TiO_2. These, in turn, might correspond to Co_3O_4 and Co_2O_3 species, implying that the cobalt present in the catalyst is not transformed into its metallic form at a calcination temperature of 300 °C. The results obtained are in agreement with most literature reports.[36,39,40]

The UV-vis spectra of the bimetallic samples are shown in the ESI† (Fig. S2). The absorbance in the visible region is significantly pronounced for the Cu–Au/TiO_2 catalyst. The broad absorption peak at around 570 nm can be ascribed to the surface plasmon resonance of Au nanoparticles. This plasmon band is sensitive to the environment and can be shifted depending on the stabilizer or the substrate. Because of the coupling between the metal nanoparticles and the TiO_2 support, the plasmon bands in almost all the bimetallic samples are red-shifted.[41]

NH_3-TPD characterization was also conducted to survey the acid strength of the Cu–Au/TiO_2 catalyst sample. Here, Cu–Au/TiO_2 was chosen for the analysis because it was found to be the most active catalyst towards the selective oxidation of cellobiose to gluconic acid. Fig. S3 in the ESI† represents the strength of the acid sites on the TiO_2 support. The peaks at high and low temperatures can be attributed to the desorption of NH_3 from the medium and weak acid sites, respectively. The high temperature desorption of ammonia is ascribed to the desorption of coordinated NH_3 bound to Lewis acid sites.[27] The peak at 261 °C is attributed to the desorption of ammonia on the weak Brønsted acid sites of the TiO_2 lattice. The Lewis acid sites contribute to the primary acidity responsible for the cellobiose and cellobionic hydrolysis, and the successive retro-aldol reaction of fructose to glycolic acid (a reaction by-product of cellobiose oxidation) in the oxidation of cellobiose to gluconic acid (Scheme 1). The total acidity estimated from the analysis of NH_3-TPD is 354.54 μmol g^{-1} which is comparable to the acid strength of TiO_2 estimated by Yang *et al.* (362 μmol g^{-1}, with a BET surface area of 79 m^2 g^{-1}).[42]

Oxidation of cellobiose

Cellobiose oxidation typically involves the hydrolysis of cellobiose to glucose as the first step. Glucose possesses 3 different types of carbons: aldehyde, primary alcohol and secondary alcohol. All three positions can be oxidized leading to different products. The oxidation of the aldehyde produces a carboxylic acid (*e.g.*, gluconic acid), whereas the oxidation of the primary and secondary alcohol affords glucuronic acid, and keto-glucose and keto-acids, respectively. An appropriately designed catalyst may greatly influence this well-studied reaction pathway. According to the HPLC results in this study, which will be discussed later in Tables 2 and 3, the observed oxidized products are mainly gluconic acid and glycolic acid, although there are other organic acids of lower-carbon containing compounds formed as a result of the decomposition or fragmentation of glucose and/or gluconic acid.

Activity and product selectivity of various monometallic and bimetallic catalysts

The effect of various monometallic and bimetallic catalysts on the conversion of cellobiose was studied under the

Table 2 Oxidative conversion of cellobiose by O_2 in H_2O over Ru–Au/TiO_2 catalyst[a]

Reaction time [h]	Cellobiose conversion [%]	Selectivity [%]				
		Glucose	Gluconic acid	Ethylene glycol	Glycolic acid	Erythritol
1	75.9	69.4	30.6	0.0	0.0	0.0
2	95.5	33.5	60.1	0.0	4.3	2.1
3	97.4	31.8	64.2	0.0	3.0	1.0
4	98.2	23.8	68.3	0.0	2.6	0.9
5	98.6	20.0	75.0	0.0	3.2	1.7
7	98.5	13.8	77.4	3.0	4.4	1.4
9	98.3	5.2	86.9	2.3	4.0	1.6
11	98.5	2.5	87.8	1.6	3.7	1.7
12	100	4.6	86.7	2.6	3.8	2.3

[a] Reaction conditions: cellobiose: 0.6 mmol, catalyst (Ru–Au/TiO_2): 0.100 g, H_2O: 20 mL, pressure (O_2): 1 MPa, temperature: 145 °C, stirring speed: 1200 rpm.

Table 3 Oxidative conversion of cellobiose by O_2 in H_2O over Cu–Au/TiO_2 catalyst[a]

Reaction time [h]	Cellobiose conversion [%]	Selectivity [%]				
		Glucose	Gluconic acid	Ethylene glycol	Glycolic acid	Cellobionic acid
1	96.7	6.0	66.1	0.0	0.0	27.9
2	98.6	9.6	70.4	0.0	0.0	20.0
3	100	11.5	88.5	0.0	0.0	0.0
4	100	0.9	86.8	4.3	8.9	0.0
5	100	0.0	81.4	7.6	11.0	0.0
7	100	0.0	68.6	11.3	15.0	0.0
9	100	0.0	58.8	17.7	22.0	0.0
11	100	0.0	43.0	27.5	26.0	0.0
12	100	0.0	41.3	28.8	25.6	0.0

[a] Reaction conditions: cellobiose: 0.6 mmol, catalyst (Cu–Au/TiO_2): 0.100 g, H_2O: 20 mL, pressure (O_2): 1 MPa, temperature: 145 °C, stirring speed: 1200 rpm.

reaction conditions described at the end of the article. The activities of the monometallic catalysts with respect to cellobiose conversion and selectivity towards gluconic acid are shown in Fig. 3. Catalytic activities are essentially similar over various catalysts, with a cellobiose conversion of about 98%. However, the product distribution and the selectivity towards gluconic acid are different. Au/TiO_2 exhibits excellent selectivity towards gluconic acid (75%), followed by Cu/TiO_2 (63%). A significant amount of formic acid (~25%) is formed over Cu/TiO_2, suggesting the superior hydrogenolysis abilities of the Cu metal as compared to Au, where C–C bonds are cleaved to yield lower carbon containing carboxylic acid compounds. On the other hand, Ru/TiO_2 shows poor selectivity towards gluconic acid, suggesting that Ru nanoparticles may not efficiently catalyze glucose oxidation to gluconic acid. Moreover, Ru catalysts have been reported to be efficient catalysts for the hydrolysis of β-1,4-glycosidic bonds.[43] Pd/TiO_2 and Co/TiO_2 catalyze cellobiose to gluconic acid with selectivities of ~25% and ~23%, respectively, along with significant amounts of glucose and fructose. The type of metal greatly influences the product distribution and particularly the selectivity towards the formation of gluconic acid. The activity of the monometallic catalysts followed the order: Au/TiO_2 > Cu/TiO_2 > Pd/TiO_2 ≈ Co/TiO_2 > Ru/TiO_2.

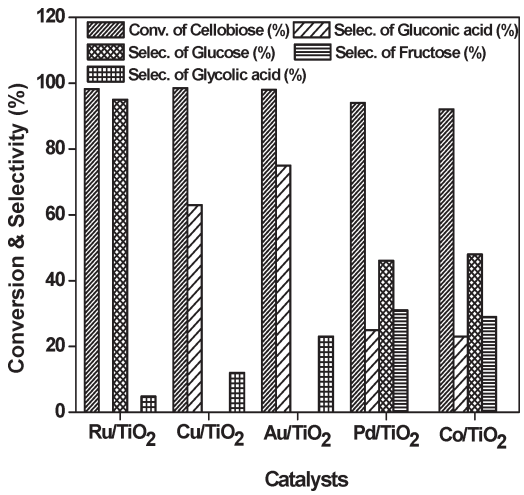

Fig. 3 Catalytic activity and product distribution of monometallic catalysts.

It has been reported in several studies[27,44] that the catalytic oxidation of cellobiose in the presence of molecular oxygen over Au nanoparticles supported on oxide supports gives rise to some conversion of cellobiose and modest selectivity towards gluconic acid. However, complete conversion of cellobiose and good selectivity towards the formation of gluconic acid over Au/TiO_2 and Au-containing bimetallic catalysts supported on TiO_2 have not yet been achieved and remain unclear. The highest conversion of cellobiose reported till date is about 96% with a gluconic acid selectivity of 63%, which was obtained by Wang *et al.*[27] using Au/TiO_2 with molecular oxygen at a pressure of 0.5 MPa and 145 °C. Additionally, An *et al.* achieved a gluconic acid selectivity of 57% over Au/TiO_2 using molecular oxygen as the oxidizing agent at 145 °C.[44] As reported in our previous work, a gluconic acid selectivity of 86.0% within 3 h over Au/TiO_2 reduced under hydrogen flow at 700 °C was achieved.[35] It was clarified that the generation of oxygen vacancies at such a high reduction temperature significantly contributed to the enhanced catalytic activity of the Au/TiO_2 catalyst. In the present study, the complete conversion of cellobiose and a gluconic acid selectivity of 88.5% are demonstrated over Cu–Au/TiO_2 prepared by the deposition–precipitation method using urea, in the presence of molecular oxygen at 145 °C in 3 h. The addition of a second metal to Au nanoparticles increases the activity and selectivity to gluconic acid by 15% compared to those of monometallic Au/TiO_2 under the same reaction conditions.

Reaction mechanism and reaction pathway investigations of individual bimetallic catalysts

To understand the reaction pathways for the conversion of cellobiose over the as-prepared bimetallic catalysts, detailed analysis of the reaction products at different times was performed and the results are shown in Tables 2–4. The selectivity patterns for gluconic acid and the distribution of products differ for all the catalysts used in this study. A

plausible reaction mechanism is proposed and shown in Scheme 1. Based on the distribution of the reaction products, as shown in Table 2, for reactions performed over the Ru–Au/TiO_2 catalyst, the pathway for the conversion of cellobiose to gluconic acid is suggested to be *via* glucose ($C_6H_{12}O_6$) as the reaction intermediate. It is proposed that (i) water molecules adsorb onto the acid site of the TiO_2 support, (ii) cellobiose then diffuses into the internal pores of TiO_2, (iii) cellobiose undergoes hydrolysis in the acid site with the adsorbed water and the hydrolysis products diffuse out of the pores, and (iv) glucose (the main reaction intermediate) is then oxidized to gluconic acid in the presence of molecular oxygen with Au–Ru nanoparticles as active sites. The gluconic acid ($C_6H_{12}O_7$) produced from glucose oxidation can further undergo decomposition or C–C, C–O and C–H bond cleavages to yield ethylene glycol, glycolic acid and erythritol, as observed in Table 2.

Table 3 illustrates the detailed distribution of the reaction products obtained over the Cu–Au/TiO_2 catalyst. It is found that cellobionic acid is formed in significant amounts (~28%) together with trace amounts of glucose (6%) in the initial reaction stage. The selectivity for cellobionic acid decreases with prolonged reaction time. The selectivity for glucose increases sharply from 6% to 11.5% at 3 h and finally decreases significantly when the reaction time reaches 4 h. The selectivity for gluconic acid, the target product, increases significantly, indicating that gluconic acid is formed from the consecutive conversion of cellobionic acid. To ascertain these phenomena, cellobiose oxidation reactions are performed over Cu–Au/TiO_2 for 15 min reaction time. Cellobionic acid and glucose selectivities of 98.2% and 1.8%, respectively, and a cellobiose conversion of 42.1% are obtained. These observations strongly suggest that the first step in cellobiose conversion over the Cu–Au/TiO_2 catalyst is the formation of cellobionic acid *via* oxidation of on glucose unit in the cellobiose structure. Glucose can be formed as a minor product through the hydrolysis of cellobionic acid catalyzed by the acid sites. The small amount of glucose observed even at prolonged reaction time suggests the ability of glucose to rapidly oxidize to gluconic acid and other degradation products such as glycolic acid and ethylene glycol. For reactions performed over Co–Au/TiO_2 and Pd–Au/TiO_2 catalysts, as shown in Tables 4 and 5, respectively, similar product distributions are observed. The slight difference is that trace amounts of xylitol and formic acid are observed at prolonged reaction times for reactions performed over Pd–Au/TiO_2. The presence of significant amounts of fructose suggests that Co–Au/TiO_2 and Pd–Au/TiO_2 catalysts promote the isomerisation of glucose to fructose and hence, fructose is seen as the reaction intermediate, a phenomenon which is different from what is observed for reactions performed over Ru–Au/TiO_2 and Cu–Au/TiO_2. The presence of both glyceraldehyde and glycolic acid suggests that fructose which is the reaction intermediate is converted to glyceraldehyde by a retro-aldol reaction. The triose fragments are subsequently converted to glycolic acid *via* the retro-aldol reaction of glyceraldehyde to glycolaldehyde and further oxidation of the latter to glycolic acid. These observations allow us to suggest that the reactions performed over Co–Au/TiO_2 and Pd–Au/TiO_2 follow the same reaction pathway, as evidenced by the presence of similar reaction products, although Pd–Au/TiO_2 reveals a better oxidizing ability because glucaric acid which is a typical over-oxidation product of gluconic acid is observed. It is noteworthy that the formation of ethylene glycol over Co–Au/TiO_2 and Pd–Au/TiO_2 is anticipated to occur *via* the decomposition of gluconic acid at an elevated reaction time. Based on these results, a plausible reaction mechanism is proposed and shown in Scheme 1. More intriguingly and interestingly, it is observed that different catalysts with different reaction times exhibit enormously different catalytic behaviours in either enhancing or suppressing the over-oxidation and decomposition of gluconic acid to other by-products, as well as the successive retro-aldol fragmentation reaction of fructose to produce glycolic acid.

Correlation between metal–metal interactions and the catalytic performance

Reactions performed over Ru–Au/TiO_2 show an increase in the selectivity for gluconic acid with time from 30.6% to 87.8% at 1 and 11 h, respectively. The XPS analysis shows the

Table 4 Oxidative conversion of cellobiose by O_2 in H_2O over Co–Au/TiO_2 catalyst[a]

Reaction time [h]	Cellobiose conversion [%]	Selectivity [%]					
		Glucose	Gluconic acid	Ethylene glycol	Glycolic acid	Glyceraldehyde	Fructose
1	91.2	29.0	22.1	0.0	0.0	0.0	48.9
2	96.3	21.0	42.7	0.0	2.3	0.0	32.2
3	96.8	0.0	33.6	4.7	18.1	10.6	28.6
4	96.9	0.0	32.1	3.2	19.5	9.1	30.7
5	97.0	0.0	30.4	8.6	30.6	16.5	9.1
7	97.0	0.0	27.1	4.9	36.1	17.0	6.2
9	97.0	0.0	25.4	10.4	30.4	21.4	5.8
11	97.1	0.0	25.5	7.3	30.2	23.5	7.0
12	97.2	0.0	24.4	7.6	28.6	26.0	6.5

[a] Reaction conditions: cellobiose: 0.6 mmol, catalyst (Co–Au/TiO_2): 0.100 g, H_2O: 20 mL, pressure (O_2): 1 MPa, temperature: 145 °C, stirring speed: 1200 rpm.

Table 5 Oxidative conversion of cellobiose by O_2 in H_2O over Pd–Au/TiO_2 catalyst[a]

Reaction time [h]	Cellobiose conversion [%]	Selectivity [%]							
		Xylitol	Gluconic acid	Ethylene glycol	Glycolic acid	Glyceraldehyde	Formic acid	Sorbitol	Fructose
1	91.2	0.0	17.3	0.0	0.0	0.0	0.0	0.0	61.2
2	96.3	0.0	29.6	0.0	10.4	2.6	0.0	0.0	33.4
3	96.8	0.0	35.6	0.0	19.3	3.2	0.0	3.9	12.7
4	96.9	0.0	36.5	5.6	24.3	8.0	0.0	4.2	0.0
5	97.0	0.0	41.8	8.6	25.2	3.0	5.0	5.5	0.0
11	97.0	2.3	5.1	21.3	34.3	2.5	11.7	9.9	0.0

[a] Reaction conditions: cellobiose: 0.6 mmol, catalyst (Pd–Au/TiO_2): 0.100 g, H_2O: 20 mL, pressure (O_2): 1 MPa, temperature: 145 °C, stirring speed: 1200 rpm.

presence of Au^0 and Ru^0, and the contact between Au and Ru atoms favours the transfer of electrons from Ru^0 towards Au^0 due to the difference in the electronegativity, resulting in a positive partial charge of Ru atoms and a negative partial charge of Au atoms.[45]

It has been postulated that for a molecule of an α,β-unsaturated aldehyde, the C=O group could be adsorbed on the Ru metal surface[45] due to the partial negative charge ($-\delta$) of the O atom. The partially oxidized second metal species strongly binds and activates the C=O group and paves the way for the selective oxidation of the C=O bonds in the aldehyde group of glucose by Au nanoparticles to yield gluconic acid. Interestingly, it has also been shown that when a second metal is added to Au, the oxidized state of the second metal (Ru^0 to RuO_2) is able to strongly interact with the support and can also function as an anchor to prevent the aggregation of gold nanoparticles.[46,47] The synergistic effect of the Ru–Au/TiO_2 catalyst contributed to the enhanced activity in selective conversion of cellobiose to gluconic acid, where partially oxidized Ru (RuO_2) interacts strongly with the aldehyde functional group of glucose, as well as with the support material to afford strong metal–support interactions, leading to highly active Au atoms for the selective oxidization of the bound-aldehyde functional group of glucose. Considering the overall energy input and cost effectiveness of designing a green approach for the production of high value-added chemicals from renewable sources, employing Ru–Au/TiO_2 as a catalyst for the oxidative conversion of cellobiose into gluconic acid may not be ideal since it requires an extended reaction time to obtain high selectivity for the product which translates into more energy input.

Reactions over Cu–Au/TiO_2 show the presence of significant amounts of glycolic acid, ethylene glycol and erythritol at extended reaction times, although it exhibits the highest activity among all the bimetallic catalysts investigated in this study. The high activity of the Cu–Au/TiO_2 catalyst in the conversion of cellobiose to gluconic acid may also be correlated with the charge transfer between the Au and Cu metal species, which has been reported to increase the availability of reactive oxygen in most oxidation reactions.[48] According to XPS analysis in this study, Cu is not fully reduced as evidenced by the presence of a CuO peak; this may therefore explain why the reactions performed over Cu–Au/TiO_2 proceed *via* cellobionic acid to gluconic acid. The formation of an Au–CuO composite structure after calcination promotes the oxidation of one glucose unit in the cellobiose structure by the lattice oxygen in the CuO framework of the Au–CuO composite structure. The consumption of the lattice oxygen in the CuO framework of the Au–CuO composite structure on the titania support creates oxygen vacancies on the copper surface. These oxygen vacancies serve as potential adsorption and activation sites for molecular oxygen. When the produced cellobionic acid is hydrolysed to gluconic acid and glucose (*via* the Lewis acid sites located on the titania support), the activated and highly reactive oxygen (O*) on the surface of Cu–Au may initiate a nucleophilic attack on glucose to produce gluconic acid. The enhanced activity of Cu–Au/TiO_2 in the selective conversion of cellobiose to gluconic acid suggests that the Au sites are accessible for the oxidation reaction and interaction with CuO that can activate molecular oxygen. According to other studies, CuO may be located on titania and at the interface between the gold particles and the titania support or as patches on the gold particles. Based on EPR, XRD and XANES results, Liu *et al.*[46] postulated that for oxidation reactions involving Cu–Au bimetallic catalysts supported on metal oxides, the catalytic structure was composed of gold particles decorated by a layer or patches of CuO, which maximized the perimeter between gold and CuO_x. The reactant adsorbed on gold would react with oxygen activated on the neighbouring CuO_x. In this way, the catalytic activity of Cu–Au/TiO_2 was greatly enhanced in comparison with that of the monometallic gold and copper. This is consistent with the fact that the plasmon band of Cu–Au/TiO_2 evolves slightly differently from that of the other bimetallic catalysts used in this study.

It has been reported that the type of metal–metal interaction and particle morphology greatly influence the reaction route.[49–51] It has also been well documented that, when Pd–Au/TiO_2 is used in oxidation reactions, *e.g.*, in the selective oxidation of alcohols and biomass-derived compounds, surface enrichment of Pd might take place, forming an Au-rich core and a Pd-rich shell. In this case, the catalytic performance of the Pd–Au bimetallic phase is actually determined by the chemical composition of the Pd-rich shell, while Au

behaves more like a promoter to prevent over-oxidation and poisoning of the Pd metal by intermediates or products. The superior catalytic performance of Pd–Au/TiO_2 in promoting the cleavage of the C–C bond by the successive retro-aldol condensation reaction of fructose to glyceraldehyde and glycolaldehyde and subsequent oxidation of the latter to glycolic acid, instead of the selective oxidation of glucose to gluconic acid, is attributed to the fact that Pd containing catalysts not only catalyze glucose isomerisation to fructose but also largely decrease the energy barrier for the retro-aldol fragmentation of fructose to trioses, *i.e.*, dihydroxyacetone and glyceraldehyde, as revealed by theoretical studies.[51,52] Furthermore, Au can disperse/isolate Pd sites, preventing oxygen poisoning of Pd in liquid-phase oxidation.[53] Au, with higher electronegativity, withdraws electrons from Pd atoms, leading to an enhanced interaction of Pd atoms with the substrate and thereby making the Pd atoms available to catalyze the isomerisation of glucose to fructose (where Pd acts as a Lewis acid catalyst),[52] evidenced by the large amount of fructose present in the product mixture, and the subsequent lowering of the energy barrier to enhance retro-aldol reactions yielding glycolic acid.

Reactions over Co–Au/TiO_2 follow the same mechanism as that observed with Pd–Au/TiO_2 because product analysis reveals substantial amounts of fructose and glyceraldehyde and also a significant amount of glycolic acid. It is important to state that the synergistic effect between gold and cobalt in catalyzing glucose isomerisation, successive retro-aldol fragmentation and further oxidation reaction to glyceraldehyde and glycolic acid is unclear and further studies to unravel the mechanistic insight are under way in our laboratory.

To gain more insights into the reaction pathway for the oxidation of cellobiose over the Cu–Au/TiO_2 catalyst in water, a number of catalytic oxidation experiments were performed using glucose, gluconic acid and fructose as the starting substrates, as shown in Table 6. In glucose conversion, the reaction pathway may involve isomerisation of glucose to fructose. The distribution of reaction products as discussed earlier shows that the rate of glucose isomerisation is highly dependent on the intrinsic nature of the bimetallic catalyst used in the reaction and the rate of glucose isomerisation controls the selectivity to glyceraldehyde (which is the main precursor to form glycolic acid). No glyceraldehyde is observed with glucose oxidation over Cu–Au/TiO_2 indicating the slow rate of glucose isomerisation to fructose, which is also evidenced by the presence of only a trace amount of fructose in the products. On the other hand, glycolic acid is produced in a significant amount while ethylene glycol is present only in trace amounts, suggesting the further decomposition or fragmentation of gluconic acid to glycolic acid and ethylene glycol. As the main product of glucose oxidation, gluconic acid is present in a large amount with a selectivity of 68% as compared to all the other by-products.

The reaction with gluconic acid as the starting compound shows a large amount of glycolic acid and ethylene glycol, confirming that glycolic acid can be produced directly from the decomposition of gluconic acid as well as small amounts of ethylene glycol. Glucaric acid is also observed, which is a typical over-oxidation product of gluconic acid. Fructose oxidation shows only a small amount of gluconic acid with a selectivity of 10.4%, while glycolic acid is formed in a comparably large amount with a selectivity of 37.7%, confirming the reaction pathway where fructose undergoes a retro-aldol reaction catalyzed by the Lewis acid sites of the TiO_2 support to form glyceraldehyde and glycolaldehyde and finally oxidation of the latter to yield glycolic acid.

A series of control experiments were also conducted to validate the presence of other C_1–C_4 compounds formed in the reaction pathway. Gluconic acid, glucose and fructose were employed as substrates in the presence of molecular O_2 at 145 °C within 3 h over the Cu–Au/TiO_2 catalyst as shown in Table 6 (entries 1–3). Reactions were also performed in the absence of a catalyst (Table 6, entries 4 and 5). The presence of a large amount of C_1–C_4 compounds (formic acid, xylitol, oxalic acid, glycolic acid and ethylene glycol) indicates that these compounds can be formed from the direct decomposition or fragmentation of glucose and fructose in the catalytic oxidation of cellobiose.[54] The absence of gluconic acid confirms that the bimetallic nanoparticles (Cu–Au) are responsible for providing the active sites for the formation of gluconic acid.

Influence of acidity or basicity on product distribution

The effect of different solvents on the distribution of reaction products and particularly on the selectivity towards gluconic

Table 6 Oxidative conversion of different biomass substrates by O_2 in H_2O over Cu–Au/TiO_2 catalyst[a]

		Selectivity [%]										
Substrate	Conversion [%]	Fructose	Glycolic acid	Ethylene glycol	Gluconic acid	Glyceraldehyde	Formic acid	Glucose	Xylitol	Glucaric acid	Oxalic acid	Others
Glucose[a]	91.3	5.7	20.5	1.6	68.4	0.0	0.0	—	1.9	0.0	—	1.9
Gluconic acid[a]	59.0	0.0	33.9	25.3	—	0.0	0.0	0.0	0.0	11.8	0.0	29.0
Fructose[a]	90.0	10.0	37.7	10.8	10.4	6.6	21.6	2.0	0.0	0.0	0.0	—
Glucose[b]	88.9	51.4	5.5	6.4	0.0	0.0	28.6	—	4.2	0.0	3.9	—
Fructose[b]	95.2	—	16.0	2.2	0.0	0.0	15.0	43.3	6.1	0.0	6.8	—

[a] Reaction conditions: cellobiose: 0.6 mmol, catalyst (Cu–Au/TiO_2): 0.100 g, H_2O: 20 mL, pressure (O_2): 1 MPa, temperature: 145 °C, stirring speed: 1200 rpm. [b] Glucose and fructose: no catalyst, H_2O: 20 mL, pressure (O_2): 1 MPa, temperature: 145 °C, stirring speed: 1200 rpm.

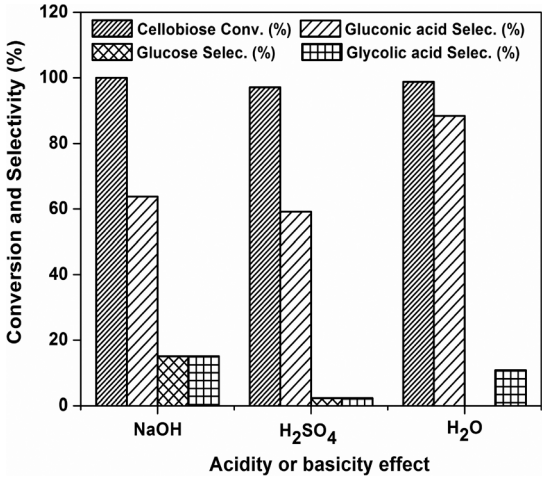

Fig. 4 Effect of acidity or basicity on cellobiose oxidation. Reaction conditions: cellobiose: 0.6 mmol, catalyst (Cu–Au/TiO_2): 0.100 g, H_2O: 20 mL, pressure (O_2): 1 MPa, temperature: 145 °C, stirring speed: 1200 rpm.

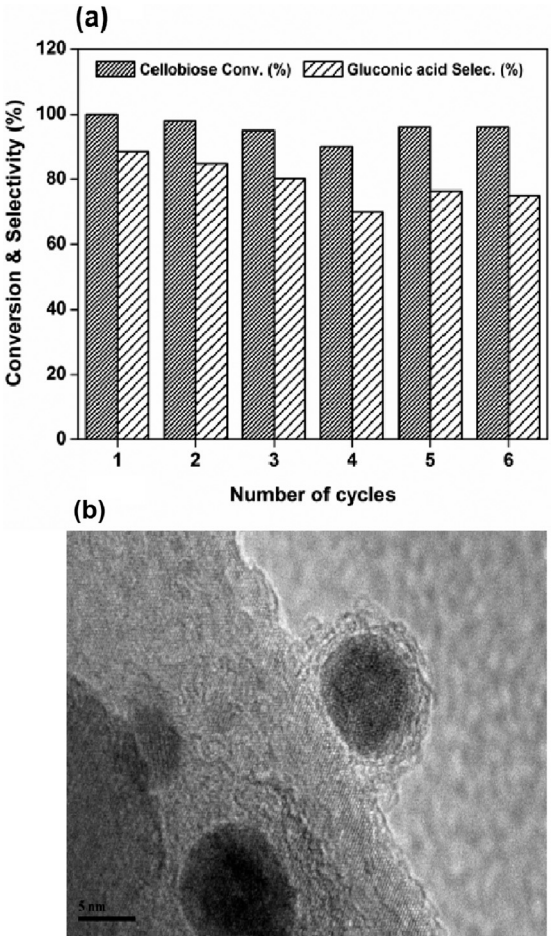

Fig. 5 (a) Recycling of Cu–Au/TiO_2 for oxidative conversion of cellobiose. Reaction conditions: cellobiose: 0.6 mmol, catalyst (Cu–Au/TiO_2): 0.100 g, H_2O: 20 mL, pressure (O_2): 1 MPa, temperature: 145 °C, stirring speed: 1200 rpm. (b) Representative TEM image of the spent Au–Cu/TiO_2 after post-treatment at 400 °C.

acid was also investigated and the results are shown in Fig. 4. Reactions performed in DI water were benchmarked against those performed in NaOH (pH of 9) and H_2SO_4 (pH of 5) aqueous solutions. A complete conversion is observed for the reactions performed in NaOH solution at 2 h and 145 °C, and the reaction products are composed of a mixture of C_2–C_6 organic compounds. The alkaline environment of the reaction medium does not favour high selectivity for gluconic acid possibly due to the fact that the degradation of gluconic acid to other lower carbon containing organic acids like glycolic acid is slightly more pronounced under basic conditions. This is evidenced by the high selectivity for glycolic acid formed in the presence of alkaline medium. Whereas, only traces of glucose and glycolic acid are observed for the reaction performed in H_2SO_4 together with a fructose selectivity of 35.9%. Therefore, it appears that the bimetallic Cu–Au/TiO_2 can catalyze the oxidation of cellobiose into gluconic acid more efficiently in neutral water, based on the results shown in Fig. 4. The promotional effect of H_2O in aiding molecular oxygen adsorption and activation on the TiO_2 support in several oxidation reactions has been well investigated and documented by several theoretical and DFT calculations.[55–57] This important phenomenon can explain why reactions performed in water medium results in a higher selectivity for gluconic acid.

Catalyst reusability

Reusability is also a key factor in heterogeneous catalysis. The results indicate that the selectivity for gluconic acid gradually decreased to 70% after the 4th cycle (Fig. 5a). It is noticed that the colour of the catalyst changed from purple to deep brown, indicating an accumulation of possible humins or carboxylic acid by-products on the surface of the catalyst over time, possibly causing deactivation. Therefore, post-treatment of the catalyst was performed by calcination at 400 °C for 1 h. The purple colour of the catalyst is restored, and the selectivity for gluconic acid reverts to 76.4% after the 5th cycle and remains almost unchanged after the 6th cycle (75%). It is worth noting that the post-treatment of the spent catalyst at 400 °C may generate CuO_x that segregates on the surface of the bimetallic nanoparticles. This phenomenon accounts for the enhanced activity and the increase in the selectivity for gluconic acid after the 5th cycle. TEM analysis (Fig. 5b) of the spent catalysts confirmed the segregation of amorphous CuO_x on the surface of the bimetallic nanoparticles. These CuO_x species served as activation sites for molecular oxygen and water reduction, which are critical for oxidation reactions.

In summary, reactions performed over the Ru–Au/TiO_2 bimetallic catalyst exhibit lower catalytic activity and selectivity towards gluconic acid in an initial reaction time of 1 to 4 h, compared to that of Cu–Au/TiO_2. Nonetheless, at extended reaction times (up to 12 h), Ru–Au/TiO_2 is able to catalyze the oxidation of cellobiose to gluconic acid with a maximum selectivity of 87% at 9 h with no significant change in the

selectivity from 9 to 12 h. This interesting observation suggests that Ru serves as a non-active oxophilic promoter protecting gold from over-oxidation. This helps in limiting the formation of by-products, and glucose (being the main reaction intermediate in the Ru–TiO_2 catalyzed reaction) is then selectively converted to gluconic acid. The use of Co–Au/TiO_2 and Pd–Au/TiO_2 bimetallic catalysts does not favour the formation of gluconic acid, although both catalysts show enhanced activities. Product analysis shows the presence of significant amounts of C_4, C_3 and C_2 organic acids, indicating the superior ability of Co–Au/TiO_2 and Au–Pd/TiO_2 in performing C–O, C–C and C–H bond cleavages.

Catalyst preparation by deposition–precipitation with urea

In a typical experiment, 1.0 g of TiO_2 was dispersed in 50 mL of 4.2 M urea aqueous solution under vigorous stirring. Appropriate amounts of gold, ruthenium and copper precursors were added to the suspension to yield 1 wt% gold, ruthenium and copper, respectively, in the monometallic catalysts. For Au-containing bimetallic samples, an Au concentration of 0.5 wt% and Cu, Co, Ru, Pd and Ni at 0.5 wt% each were mixed to obtain 1 wt% total metal loading on the catalyst support. The temperature of each suspension was increased to 80 °C, and each suspension was stirred for 6 h to enable slow decomposition of urea to ammonia, which then resulted in an increased pH and consequently slow precipitation of the metallic particles. The solids were finally recovered by filtration and washed thoroughly with deionised water (DI), in order to ensure complete removal of chlorine residues. Thereafter, the solids were dried overnight in an oven at 90 °C and finally calcined at 300 °C in air. The calcined samples were then stored in desiccators to avoid any adverse effects of light or atmospheric contaminants.

Catalyst characterization

Powder X-ray diffraction (XRD) patterns were recorded on a Bruker AXS D8 diffractometer under ambient conditions using Cu Kα radiation (λ = 0.15406 nm) from a Cu X-ray tube operated at 40 kV and 40 mA. The diffractograms were recorded in the 2θ range of 10–90°, in steps of 0.02° with a count time of 20 s at each point. Prior to the test, the samples were dried at 80 °C overnight.

Textural properties were determined by nitrogen physisorption using a Micromeritics TriStar apparatus. The specific area was calculated using the Brunauer–Emmett–Teller (BET) equation and the pore size distribution was analyzed with the Barrett–Joyner–Halenda (BJH) method.

The samples were also analyzed by X-ray photoemission spectroscopy (XPS). XPS spectra were collected with a Thermo Escalab 250 spectrometer. Spectra were recorded using an Al anode (Al Kα = 1486.6 eV) with a 20 eV pass energy, 0.1 eV energy step and 0.1 s dwelling time. Energy corrections were performed using C1s (284.6 eV) as a reference.

The morphology and particle size were determined by transmission electron microscopy (TEM) using a JEOL JEM-2100F, operating at an accelerating voltage of 200 keV. For the TEM analysis, the samples were dispersed by ultrasonication in ethyl alcohol for 30 min and a drop of the supernatant liquid was placed onto a holey carbon film supported on a copper grid.

XRF (with a Bruker AXS S4 Explorer) analysis was also performed on the samples to confirm the metal loading present.

The UV-vis spectra of the synthesized catalysts were recorded in the scan range of 210–900 nm, using a UV-visible spectrophotometer (Shimadzu model UV-2450; Shimadzu, Kyoto, Japan) equipped with an integrating sphere, with $BaSO_4$ as the reference.

Temperature programmed desorption of NH_3 (NH_3-TPD) was performed on a Micromeritics AutoChem 2920 apparatus. 200 mg of the catalyst was placed into a quartz U-tube, heated for 2 h at 600 °C in Ar, and then kept at 100 °C for NH_3 adsorption. When saturated adsorption was achieved, the system was swept with He for 3 h. Then the temperature was programmed to increase to 600 °C under a heating rate of 10 °C min^{-1}. The desorbed NH_3 was analyzed by using a TCD detector.

Reaction setup and product analysis

Oxidation of cellobiose was carried out in a 50 mL Teflon-lined capacity batch reactor (PARR instrument) under reaction conditions of 145 °C, 20 mL of DI H_2O at 2 h, unless otherwise stated. Cellobiose (typically 0.600 mmol) and the catalyst (0.100 g) were added into the reactor pre-charged with DI water. The system was charged with pure O_2 at a controlled pressure, after removing air by pressurizing and depressurizing several times with pure O_2. The reaction was performed under different reaction conditions with steady stirring (1200 rpm). After the reaction, the products were analyzed by a liquid chromatograph equipped with a RID-6A refractive index detector and a Hi-Plex H (300 × 6.5 mm) column with 0.01 M H_2SO_4 acid solution as the mobile phase (flow rate of 1 mL min^{-1}).

Cellobiose conversion is defined as:

$$X_g = \frac{C_{g,0} - C_g}{C_{g,0}} \quad (1)$$

where C_g is the concentration of cellobiose after a certain reaction time and $C_{g,0}$ is the initial cellobiose concentration.

Product selectivity for a compound 'p' is defined as:

$$S_g = \frac{C_p}{C_{g,0} - C_g} \quad (2)$$

where C_p is the concentration of a product after a certain reaction time.

Conclusions

Cellobiose can be converted to gluconic acid with 88.5% selectivity and 100% conversion if the reaction is catalyzed by

Cu–Au/TiO_2 at 145 °C and an O_2 pressure of 1.0 MPa within a reaction time of 3 h. The M–Au/TiO_2 bimetallic catalysts, with M = Ru, Cu, Co and Pd, used in this study interestingly showed different catalytic behaviours in converting cellobiose to gluconic acid. The conversion of cellobiose to gluconic acid, catalyzed by Cu–Au/TiO_2, involves (i) the transformation of cellobiose into cellobionic acid *via* the oxidation of one glucose unit in the cellobiose structure, (ii) the hydrolysis of the β-1,4 glycosidic bond in cellobionic acid to gluconic acid and glucose, and (iii) glucose oxidation to gluconic acid. At extended reaction times, gluconic acid is converted to smaller carbon-containing carboxylic acids. Reactions over Ru–Au/TiO_2 revealed that glucose was the reaction intermediate, which is oxidized to gluconic acid. However, kinetics of the conversion of cellobiose to gluconic acid over Ru–Au/TiO_2 is slower than that over Cu–Au/TiO_2. Reactions performed over Co–Au/TiO_2 and Pd–Au/TiO_2 revealed fructose as the reaction intermediate, promoting the successive retro-aldol condensation reactions of fructose to glycolic acid. The recycled Cu–Au/TiO_2 also showed appreciable amounts of gluconic acid suggesting the superior stability of the reused catalyst even after four cycles. The use of neutral water as the reaction solvent proved to be much more efficient than using acidic or basic reaction medium. Lastly, the enhanced activity, selectivity and stability of the Au–Cu/TiO_2 bimetallic catalyst are due to the metal–metal interactions caused by the redox properties of the Cu metal species.

Acknowledgements

This project is funded by the National Research Foundation (NRF), Prime Minister's Office, Singapore under its Campus for Research Excellence and Technological Enterprise (CREATE) program. The authors also gratefully acknowledge support from the Singapore Agency for Science, Technology and Research (A*STAR) for releasing grants for this research.

Notes and references

1 J. N. Chheda, G. W. Huber and J. A. Dumesic, *Angew. Chem., Int. Ed.*, 2007, **46**, 7164–7183.
2 A. Corma, S. Iborra and A. Velty, *Chem. Rev.*, 2007, **107**, 2411–2502.
3 D. A. Simonetti and J. A. Dumesic, *Catal. Rev.: Sci. Eng.*, 2009, **51**, 441–484.
4 S. Van de Vyver, J. Geboers, P. A. Jacobs and B. F. Sels, *ChemCatChem*, 2011, **3**, 82–94.
5 J. A. Geboers, S. Van de Vyver, R. Ooms, B. Op de Beeck, P. A. Jacobs and B. F. Sels, *Catal. Sci. Technol.*, 2011, **1**, 714–726.
6 B. Girisuta, L. P. B. M. Janssen and H. J. Heeres, *Chem. Eng. Res. Des.*, 2006, **84**, 339–349.
7 S. Govindaswamy and L. M. Vane, *Bioresour. Technol.*, 2010, **101**, 1277–1284.
8 S. Naik, V. V. Goud, P. K. Rout and A. K. Dalai, *Renewable Sustainable Energy Rev.*, 2010, **14**, 578–597.
9 H. Zhao, J. E. Holladay, H. Brown and Z. C. Zhang, *Science*, 2007, **316**, 1597–1600.
10 A. Mirescu and U. Prüße, *Appl. Catal., B*, 2007, **70**, 644–652.
11 S. Biella, L. Prati and M. Rossi, *J. Catal.*, 2002, **206**, 242–247.
12 X. Tan, W. Deng, M. Liu, Q. Zhang and Y. Wang, *Chem. Commun.*, 2009, 7179–7181.
13 B. Kamm, *Angew. Chem., Int. Ed.*, 2007, **46**, 5056–5058.
14 H. Wang, L. Zhu, S. Peng, F. Peng, H. Yu and J. Yang, *Renewable Energy*, 2012, **37**, 192–196.
15 V. R. Choudhary, D. K. Dumbre and S. K. Bhargava, *Ind. Eng. Chem. Res.*, 2009, **48**, 9471–9478.
16 C. Della Pina, E. Falletta and M. Rossi, *J. Catal.*, 2008, **260**, 384–386.
17 T.-C. Ou, F.-W. Chang and L. S. Roselin, *J. Mol. Catal. A: Chem.*, 2008, **293**, 8–16.
18 L. Leite, V. Stonkus, K. Edolfa, L. Ilieva, D. Andreeva, L. Plyasova, J. W. Sobczak, S. Ionescu and G. Munteanu, *J. Mol. Catal. A: Chem.*, 2004, **215**, 95–101.
19 F.-W. Chang, L. S. Roselin and T.-C. Ou, *Appl. Catal., A*, 2008, **334**, 147–155.
20 E. V. Murzina, A. V. Tokarev, K. Kordás, H. Karhu, J.-P. Mikkola and D. Y. Murzin, *Catal. Today*, 2008, **131**, 385–392.
21 J. Kuusisto, A. V. Tokarev, E. V. Murzina, M. U. Roslund, J.-P. Mikkola, D. Y. Murzin and T. Salmi, *Catal. Today*, 2007, **121**, 92–99.
22 W.-C. Li, M. Comotti and F. Schüth, *J. Catal.*, 2006, **237**, 190–196.
23 F.-W. Chang, T.-C. Ou, L. S. Roselin, W.-S. Chen, S.-C. Lai and H.-M. Wu, *J. Mol. Catal. A: Chem.*, 2009, **313**, 55–64.
24 H.-Y. Lin and Y.-W. Chen, *Ind. Eng. Chem. Res.*, 2005, **44**, 4569–4576.
25 P. Serna, P. Concepción and A. Corma, *J. Catal.*, 2009, **265**, 19–25.
26 M. Conte, A. F. Carley, G. Attard, A. A. Herzing, C. J. Kiely and G. J. Hutchings, *J. Catal.*, 2008, **257**, 190–198.
27 D. An, A. Ye, W. Deng, Q. Zhang and Y. Wang, *Chem. – Eur. J.*, 2012, **18**, 2938–2947.
28 J. Zhang, X. Liu, M. N. Hedhili, Y. Zhu and Y. Han, *ChemCatChem*, 2011, **3**, 1294–1298.
29 A. Venugopal, J. Aluha and M. Scurrell, *Catal. Lett.*, 2003, **90**, 1–6.
30 B. Pawelec, A. M. Venezia, V. La Parola, S. Thomas and J. L. G. Fierro, *Appl. Catal., A*, 2005, **283**, 165–175.
31 R. Zanella, L. Delannoy and C. Louis, *Appl. Catal., A*, 2005, **291**, 62–72.
32 S. Ajaikumar, M. Golets, W. Larsson, A. Shchukarev, K. Kordas, A. R. Leino and J. P. Mikkola, *Microporous Mesoporous Mater.*, 2013, **173**, 99–111.
33 S. Ajaikumar, J. Ahlkvist, W. Larsson, A. Shchukarev, A. R. Leino, K. Kordas and J. P. Mikkola, *Appl. Catal., A*, 2011, **392**, 11–18.
34 A. Sandoval, C. Louis and R. Zanella, *Appl. Catal., B*, 2013, **140–141**, 363–377.
35 P. N. Amaniampong, K. Li, X. Jia, B. Wang, A. Borgna and Y. Yang, *ChemCatChem*, 2014, **6**, 2105–2114.
36 Z. Jiang, W. Zhang, L. Jin, X. Yang, F. Xu, J. Zhu and W. Huang, *J. Phys. Chem. C*, 2007, **111**, 12434–12439.

37 R. J. Chimentão, F. Medina, J. L. G. Fierro, J. Llorca, J. E. Sueiras, Y. Cesteros and P. Salagre, *J. Mol. Catal. A: Chem.*, 2007, **274**, 159–168.
38 W. Huang, Z. Zuo, P. Han, Z. Li and T. Zhao, *J. Electron Spectrosc. Relat. Phenom.*, 2009, **173**, 88–95.
39 R. C. King, J. F. Moulder and J. Chastain, *Handbook of X-ray photoelectron spectroscopy: a reference book of standard spectra for identification and interpretation of XPS data*, Physical Electronics, Eden Prairie, Minn, 1992.
40 J.-Y. Zheng, J.-B. Pang, K.-Y. Qiu and Y. Wei, *Microporous Mesoporous Mater.*, 2001, **49**, 189–195.
41 X. Li, T. Fan, H. Zhou, B. Zhu, J. Ding and D. Zhang, *Microporous Mesoporous Mater.*, 2008, **116**, 478–484.
42 M. Yang, Y. Men, S. Li and G. Chen, *Appl. Catal., A*, 2012, **433–434**, 26–34.
43 T. Komanoya, H. Kobayashi, K. Hara, W.-J. Chun and A. Fukuoka, *J. Energy Chem.*, 2013, **22**, 290–295.
44 D. An, A. Ye, W. Deng, Q. Zhang and Y. Wang, *10th European Congress on Catalysis, EUROPACAT-X*, Glasgow, Scotland, 2011.
45 L. N. Protasova, E. V. Rebrov, T. S. Glazneva, A. Berenguer-Murcia, Z. R. Ismagilov and J. C. Schouten, *J. Catal.*, 2010, **271**, 161–169.
46 X. Liu, A. Wang, L. Li, T. Zhang, C.-Y. Mou and J.-F. Lee, *J. Catal.*, 2011, **278**, 288–296.
47 X. Liu, A. Wang, X. Yang, T. Zhang, C.-Y. Mou, D.-S. Su and J. Li, *Chem. Mater.*, 2008, **21**, 410–418.
48 L. Chmielarz, R. Dziembaj, T. Grzybek, J. Klinik, T. Łojewski, D. Olszewska and A. Węgrzyn, *Catal. Lett.*, 2000, **70**, 51–56.
49 A. Wang, X. Y. Liu, C.-Y. Mou and T. Zhang, *J. Catal.*, 2013, **308**, 258–271.
50 Y. Chen, H. Wang, C.-J. Liu, Z. Zeng, H. Zhang, C. Zhou, X. Jia and Y. Yang, *J. Catal.*, 2012, **289**, 105–117.
51 W. Deng, Q. Zhang and Y. Wang, *Catal. Today*, 2014, **234**, 31–41.
52 W. Dedsuksophon, K. Faungnawakij, V. Champreda and N. Laosiripojana, *Bioresour. Technol.*, 2011, **102**, 2040–2046.
53 A. N. Kholodovich, P. A. Simonov, R. I. Kvon, A. V. Bukhtiyarov, V. I. Zaikovskii, Y. A. Chesalov and A. V. Romanenko, *Kinet. Catal.*, 2008, **49**, 886–892.
54 L. Xin, Z. Zhang, J. Qi, D. Chadderdon and W. Li, *Appl. Catal., B*, 2012, **125**, 85–94.
55 L. Liu, B. McAllister, H. Ye and P. Hu, *J. Am. Chem. Soc.*, 2006, **128**, 4017–4022.
56 A. Bongiorno and U. Landman, *Phys. Rev. Lett.*, 2005, **95**, 106102.
57 O. Pozdnyakova-Tellinger, D. Teschner, J. Kröhnert, F. C. Jentoft, A. Knop-Gericke, R. Schlögl and A. Wootsch, *J. Phys. Chem. C*, 2007, **111**, 5426–5431.